Article

JOURNAL OF COMPOSITE MATERIALS

Journal of Composite Materials
2023, Vol. 57(1) 63–78

DOI: 10.1177/00219983221137925
journals.sagepub.com/home/jcm
SAGE

Uncertainty quantification in elastic constants of SiC_f/SiC_m tubular composites using global sensitivity analysis

Hemanth Thandaga Nagaraju[1], James Nance[2], Nam H Kim[1], Bhavani Sankar[1] and Ghatu Subhash[1]

Abstract

Silicon carbide fiber and silicon carbide matrix (SiC_f/SiC_m) tubes produced through the chemical vapor infiltration process have become a candidate cladding material in nuclear applications. The performance of this composite is influenced by many variables such as braiding angle, porosity, material properties, etc., which vary over a range of values due to the inherent fluctuations in the manufacturing process. In this study, the variability in elastic constants of SiC_f/SiC_m composite has been quantified through multiscale finite element (FE) simulations, variable screening, and high-fidelity surrogate modeling. The key variables dominantly affecting the elastic constants of SiC_f/SiC_m tubes were identified using global sensitivity analysis. A surrogate to the high-fidelity FE-based model was used in Monte Carlo simulations to generate a hundred thousand samples from which the uncertainty in elastic constants was assessed. It turned out that the coefficient of variation was less than 10%.

Keywords

multi-scale finite element analysis, silicon carbide composites, global sensitivity analysis, uncertainty quantification, monte-carlo simulations

Introduction

Since the Fukushima Daiichi nuclear accident in 2011,[1] there have been accelerated efforts to develop accident-tolerant fuels (ATF) to enhance the safety and reliability of light water reactors (LWR).[2] In conditions that occurred during the Fukushima accident, known as the loss of coolant accident (LOCA), it is speculated that the temperature inside the nuclear reactor core may have exceeded 1000°C. At such high temperatures, the currently used Zircaloy material is known to undergo significant degradation in the form of loss of ductility, loss of creep resistance, rapid oxidation, hydride formation, and oxide layer spallation.[3–5] Efforts to identify alternate accident-tolerant materials have focused on silicon carbide fiber and silicon carbide matrix composites (SiC_f/SiC_m) manufactured through mechanical braiding of SiC fibers followed by chemical vapor infiltration (CVI) of the SiC matrix. These composites have impressive characteristics such as low neutron cross-section, low coefficient of thermal expansion, and high elastic modulus.[6,7] Moreover, SiC_f/SiC_m composite has been engineered to exhibit pseudo ductility and improved fracture toughness, unlike the monolithic SiC.[8] These properties make the SiC_f/SiC_m composite an attractive candidate to replace Zircaloy as a cladding material.[8]

However, these composites exhibit significant variability in their microstructural features (e.g., porosity distribution, fiber diameter, yarn angle, wall thickness) and mechanical properties (e.g., Young's modulus, shear modulus, and Poisson's ratio) all of which can lead to uncertainty in the performance of the composite during service conditions. Uncertainties are typically classified into *aleatory* (representing variability) and *epistemic* (lack of knowledge). For the current analysis, the aleatory uncertainty can be due to the variability in microstructure, geometry, and material properties discussed above. Additional variability comes

[1]University of Florida, Department of Mechanical and Aerospace Engineering, Gainesville, FL, USA
[2]University of Florida, Department of Material Science and Engineering, Gainesville, FL, USA

Corresponding author:
Nam H Kim, Department of Mechanical and Aerospace Engineering, University of Florida, POBox 116250, Gainesville, FL 32611-6250, USA.
Email: nkim@ufl.edu

from the manufacturing process (variation in thickness, porosity, imperfections in weave angles, etc.) and the variability due to operating conditions (e.g., operating temperature). Epistemic uncertainty stems from limited knowledge of the statistical distribution that governs the elastic constants of the composite and is due to the limited number of samples that can be tested to get statistical information. The uncertainty can be *(i) type of distribution* (e.g., normal, lognormal, or Weibull), *(ii) parameters of the distribution*, such as mean and standard deviation in the case of the normal distribution, and *(iii) measurement uncertainty* associated with the fact that measurements are of finite accuracy. Specific to this SiC_f/SiC_m composite,[9] variability in individual SiC fiber properties and the CVI SiC matrix have been documented. The residual porosity of the SiC_f/SiC_m composite and its distribution, which is difficult to characterize, forms a major source of epistemic uncertainty. Although experiments carried out by various researchers have helped determine the range of elastic constants of SiC_f/SiC_m composite tubes,[7] there have been limited studies to identify the distribution of mechanical properties of SiC_f/SiC_m tubes. In this paper, we intend to identify the distribution of elastic constants of SiC_f/SiC_m tubes and quantify the concomitant coefficient of variation (CV) which will help model the performance of SiC_f/SiC_m cladding material in nuclear applications.

Despite the advances in testing and ultrasonic measurements of ceramic matrix composites,[10–12] the identification of the above distribution of properties and geometric variables demands a prohibitively large number of SiC_f/SiC_m specimens and experiments. Additionally, it is impractical to test the performance of SiC_f/SiC_m cladding material at every possible combination of loads. Alternatively, a finite element (FE) based model can handle a complicated combination of loads compared to the simple uniaxial loads often used in experiments. Furthermore, it is practically impossible to control the values of relevant variables (such as porosity, Young's modulus, Poisson's ratio, braiding angle, and others) in the manufacturing process while these quantities can be precisely accounted for in a numerical model. Such an investigation can help decipher the relationships between the input variables and elastic constants of the composite. A two-scale homogenization is generally adapted to analyze textile composites[13,14] in FE-based micromechanics. The microscale homogenization involves the analysis of SiC yarn and the subsequent mesoscale analysis is concerned with textile composites. The SiC_f/SiC_m composites have been analyzed by Yamada et al.[15] to study the thermal diffusivity and thermal conductivity. The effects of porosity on unidirectional SiC yarn were studied by Chateau et al.[16] by assigning negligible stiffness values to finite elements representing voids in the FE mesh of the volume element. In this study, we have developed an FE-based multiscale methodology to evaluate the effective elastic constants of the SiC_f/SiC_m composites acknowledging their key features such as tubular geometry, residual porosity, and high yarn volume fractions. The developed FE methodology is used to identify the distributions of elastic constants of SiC_f/SiC_m composites, namely Young's moduli in the circumferential and longitudinal directions, Poisson's ratio, and shear modulus.

The uncertainty quantification in elastic constants of SiC_f/SiC_m composite tubes is challenging due to the variabilities in microstructure and properties at different length scales. The variability is present at the individual fiber level (material properties) at the yarn level (intrayarn microporosity and yarn properties), and at the composite level (braiding angle, macroporosity, and volume fraction). Therefore, it is necessary to include in the numerical models, different scales to represent the effect of uncertainty at corresponding scales.[17,18]

The second challenge is the computational cost involved in uncertainty quantification, which usually requires hundreds of thousands of simulations. There are various methods available for reducing the computational cost in uncertainty quantification, such as surrogate modeling,[19,20] importance sampling,[21–23] local expansion-based method,[24,25] polynomial chaos expansion,[26–28] etc. Since comparing different methods is out of scope, surrogate modeling through a polynomial response surface is used in this research. However, the proposed methodology should work with other methods of uncertainty quantification as well.

The last but not the least of the identified challenges is the ubiquitous 'curse of dimensionality'. Even if the surrogate model can be efficient to generate hundreds of thousands of samples for uncertainty quantification, it can still be expensive to build a high-fidelity surrogate model of sufficient predictive accuracy, especially when the number of input variables is high, which is called the curse of dimensionality.[29] Moreover, varying some of the variables (such as yarn cross-sectional area, fiber volume fraction, and braiding angle) is an arduous task in FE simulations as changing these variables demands the generation of a new FE mesh. In practice, however, not all input variables significantly affect the uncertainty in elastic constants of SiC_f/SiC_m composites. Therefore, it is possible to screen out the input variables that do not have a significant contribution to the output uncertainty. In this research, global sensitivity analysis (GSA) is utilized to downselect dominant input variables. GSA has been used to decompose the uncertainty of the model output into the different sources in the model inputs.[30,31] Among many GSA methods, variance-based sensitivity methods are formulated based on conditional variance, and sensitivities can be assessed by Monte Carlo simulation or Latin Hypercube Sampling (LHS).[32] The Fourier amplitude sensitivity test indices[33,34] and the Sobol

indices[35–37] are commonly used to compute the sensitivity indices, and we chose the latter in this study.

This paper is organized as follows. In 'Methodology', various methods that have been used in this study are presented, including the Mori-Tanaka method to account for porosity, analytical and numerical methods of homogenization, global sensitivity analysis, surrogate modeling, and uncertainty quantification using Monte Carlo simulation. The 'Results and discussions' include validation of FE-based homogenization of SiC_f/SiC_m composites and fitting the distribution of elastic constants using the Johnson distributions. This is followed by 'Conclusions'.

Methodology

Overview of the approach

A bird's eye view of the methods/models used in this study is schematically shown in Figure 1. The material properties of the constituent SiC matrix were degraded to account for porosity. The details of degrading the material properties through the Mori-Tanaka method can be found later in this section. The first task was to identify the significant variables influencing the elastic constants. For this purpose, an analytical model called BraidCAM (discussed later) was used to calculate the effective elastic constants. The predictions from the analytical model were used in global sensitivity analysis to rank the input variables based on their first-order Sobol indices.[35–37] The FE simulations are executed by varying the identified dominant input variables and keeping the insignificant variables at their mean values (or arbitrarily chosen constant values). The multiscale FE methodology to calculate the effective elastic constants of SiC_f/SiC_m composite tubes accounting for their nuances such as tubular geometry and high yarn volume fraction is explained in this section while the results of FE simulations are verified with those of experiments in results and discussions.

Often, some of the assumptions in analytical models are driven by computational convenience rather than governing physics and consequently, their predictions might be consistently different from those of experiments. The chosen analytical model in this study called BraidCAM, consistently predicts higher values of elastic constants than experiments.[7] Though the results of BraidCAM are not in agreement with the experiments, the analytical model is still useful as its results are strongly correlated with FE simulations as demonstrated in the results and discussions section for the same

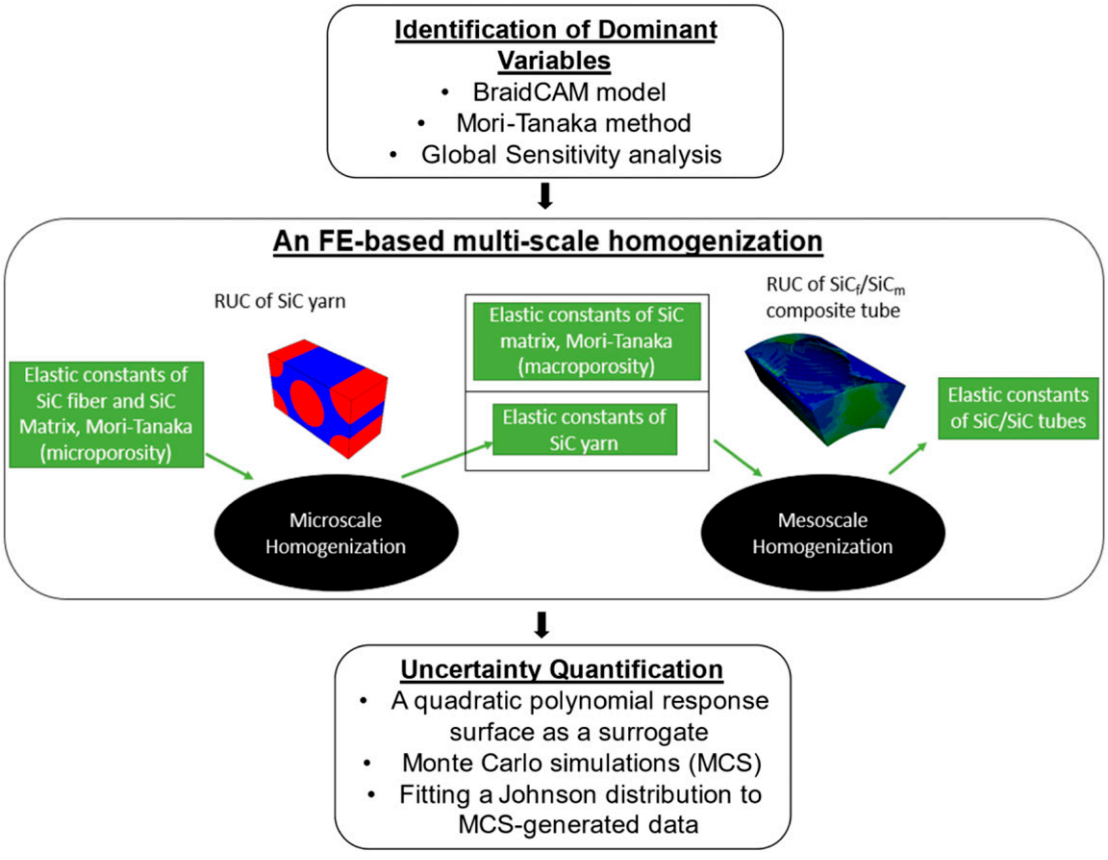

Figure 1. A bird's eye view of the methods/models used in this study. RUC stands for the repeatable unit cell.

values of dominant input variables. Thus, the quick computing BraidCAM model was used in the sensitivity analysis. The FE simulations can then be executed by varying only the dominant input variables identified in sensitivity analyses. Although accurate, FE simulations are time-consuming, and it may not be feasible to execute hundreds of thousands of simulations due to limitations in computational resources. Hence, a polynomial response surface was used as a surrogate for FE simulation. This polynomial regression is explained in the later part of this section. The so-constructed polynomial response surface was used in Monte Carlo simulations (MCS) to calculate the effective elastic constants at random values of dominant earlier. Once we have large data of elastic constants, a Johnson distribution was fit that matches the statistics of MCS-generated data. The uncertainty in elastic constants is then quantified by calculating the coefficient of variation (CV).

Application of Mori-Tanaka method to SiC_f/SiC_m textile composite

One of the salient microstructural features of SiC_f/SiC_m composites is residual porosity. The existing literature indicates the residual porosity in CVI SiC_f/SiC_m composites to be about 8%–17%.[7] During the CVI process, the SiC vapor which deposits as the matrix material fails to reach all the space between the fibers, resulting in residual porosity. The pores that are found within a yarn are called intrayarn micropores. The fraction of void volume of intrayarn micropores with respect to the volume of yarn is termed intrayarn microporosity (ϕ^{micro}). The pores formed between the yarns are called macropores whose fraction (with respect to the volume of the composite) is represented by macroporosity (ϕ^{macro}). Though this distinction can be found in the literature,[38,39] there are not many characterization studies that state the exact numerical values for intrayarn microporosity and macroporosity as it is difficult to differentiate between the yarn region and matrix region, and hence, researchers often state the overall porosity of the composite tubes in their works.[40,41] The shape of the pores could be complex and irregular, and their distribution could be different even at the same level of overall porosity, which makes it difficult to explicitly model the pores in FE analyses.

In this study, we used the Mori-Tanaka method[42–44] to account for the effect of pores in the SiC_f/SiC_m composite. Considering the stiffness tensor of the trapped voids as zeros, the stiffness tensor of the material system C^{mt} is given by[45]

$$C^{mt} = (1-\psi_v).C_{base} : \left[(1-\psi_v).I + \psi_v (I-Y)^{-1}\right]^{-1} \quad (1)$$

where ψ_v is the void volume fraction, C_{base} is the stiffness tensor of the material surrounding the pores, I is the fourth order tensor, and Y is the Eshelby tensor that depends on the shape of the voids. For spherical voids, it is given by[44]

$$Y_{ijkl} = \frac{5v-1}{15(1-v)}\delta_{ij}\delta_{kl} + \frac{4-5v}{15(1-v)}\left(\delta_{ik}\delta_{jl} + \delta_{il}\delta_{jk}\right) \quad (2)$$

where v is the Poisson's ratio of the material surrounding the pores and δ is the Kronecker delta. In microscale homogenization, the elastic properties of the SiC matrix within the yarn were degraded based on the estimates of microporosity, while in mesoscale homogenization, the elastic properties of the SiC matrix outside the yarn were degraded based on the estimates of macroporosity. Rohmer et al.[46] estimated the fiber volume fraction within a single yarn to be 52% and the matrix volume fraction to be 36%. By neglecting the presence of pyrolytic carbon interphase, the microporosity could be calculated as 12%, even though the architecture of the specimens considered in the current study is different from the layer-to-layer interlock architecture of the SiC_f/SiC_m tubular specimens studied by Rohmer et al.[46] In the following calculations, it is assumed that the intrayarn microporosity is constant at 12%. It was further assumed that all of the intrayarn micropores are trapped in the matrix meaning that the matrix was degraded according to equation (1) with $\psi_v = 0.25$ (the fraction of volume of pores with respect to matrix volume in the yarn) and the resulting degraded matrix properties were used as input material properties in microscale homogenization along with properties of the fiber.

The macroporosity (ϕ^{macro}) was calculated by using the following relation involving overall porosity ($\phi^{overall}$) and microporosity (ϕ^{micro}):

$$\phi^{overall} = \psi_{yarn}.\phi^{micro} + \left(1-\psi_{yarn}\right)\phi^{macro} \quad (3)$$

where ψ_{yarn} is the yarn volume fraction in the composite. The yarn volume fraction is difficult to measure from the specimens, however, Rohmer et al. studied the SiC_f/SiC_m tubes with a designed *fiber volume fraction* of 35% and the authors found the *fiber volume fraction within a single yarn* to be 52%. As the *fiber volume fraction* of the textile composite tube is the product of the *yarn volume fraction* (ψ_{yarn}) in the textile composite and *fiber volume fraction within a single yarn*, the *yarn volume fraction* can be estimated as $\psi_{yarn} = 67\%$.

The Mori-Tanaka method is used to account for both intrayarn microporosity and macroporosity in microscale and mesoscale homogenization methods, respectively. In mesoscale homogenization, since all the macro-pores are assumed to be present in the SiC matrix, the Mori-Tanaka method is utilized to calculate the degraded matrix properties to account for macroporosity. The properties of SiC_f/SiC_m composites are calculated through homogenization involving the degraded properties of the SiC matrix and that of the yarn. The homogenization methods could be analytical or based on FE simulations. Even though the analytical homogenization models are based

on simpler assumptions and may not necessarily capture all the physical phenomena, they provide results quickly compared to FE-based homogenization. Thus, the analytical homogenization model was treated as a low-fidelity model and used to identify the dominant variables influencing the elastic constants of the textile composite.

Analytical model to calculate the effective elastic constants of SiC_f/SiC_m tube

An open-source analytical model called BraidCAM, developed by Melenka et al. was adapted to estimate the elastic constants of the SiC_f/SiC_m tubular composites.[47] In this model, the stiffness tensors of each yarn and the matrix in the unit cell are transformed into the global coordinate system. The transformed global stiffness tensor of individual constituents is multiplied with corresponding volume fractions. The obtained products are then summed up to get the stiffness tensor of the braided composite. The complete details of this methodology can be found in the works of Melenka et al.[48] In the current research, the BraidCAM model was used to predict the elastic constants of the textile composite by volume averaging the stiffness of individual constituents namely, yarn and matrix.

The five independent elastic constants of a transversely isotropic SiC yarn are calculated from the elastic constants of isotropic fiber and isotropic matrix as per the following relations:

$$
\begin{aligned}
E_{1,yarn} &= \psi_f E_f + (1-\psi_f) E_m \\
E_{2,yarn} &= E_{3,yarn} = \frac{1}{\frac{\psi_f}{E_f} + \frac{(1-\psi_f)}{E_m^*}} \\
G_{12,yarn} &= \frac{1}{\frac{\psi_f}{G_f} + \frac{(1-\psi_f)}{G_m^*}} \\
\nu_{12,yarn} &= \nu_{13,yarn} = \psi_f \nu_f + (1-\psi_f)\nu_m^* \\
G_{23,yarn} &= \frac{G_m^*(\psi_f + \eta_{23}(1-\psi_f))}{\eta_{23}(1-\psi_f) + \psi_f \left(\frac{G_m^*}{G}\right)}
\end{aligned}
\tag{4}
$$

where $\eta = \frac{3-4\nu_m^* + \frac{G_m^*}{G_f}}{4(1-\nu_m^*)}$, E_f is the young's modulus of fiber, G_f is the shear modulus of fiber, ν_f is the Poisson's ratio of fiber, ψ_f is the volume fraction of fiber in SiC yarn, E_m^*, G_m^*, and ν_m^* are the degraded elastic constants of the SiC matrix based on equation (1) using an intrayarn microporosity of 12% and assuming that the pores are trapped in the matrix region as detailed earlier. The obtained elastic constants of yarn are now the input to the mesoscale homogenization of textile composite. The stiffness of the matrix, which is the other material variable, was degraded by using equation (1) but based on the macroporosity fraction obtained from equation (3). The elastic constants of the textile composite are calculated based on transformation and associated volume averaging of the stiffness of yarn and matrix in the framework of the BraidCAM model.

Global sensitivity analysis to identify the dominant variables by Sobol method

Many variables could potentially affect the elastic constants of SiC_f/SiC_m tube, such as fiber volume fraction, yarn cross-sectional area, braiding angle, Young's modulus of SiC fiber, Young's modulus of SiC matrix, Poisson's ratio of SiC fiber, Poisson's ratio of SiC matrix, and porosity. It is difficult to track the problem in such a high-dimensional input space. Therefore, a sensitivity analysis was carried out to determine the rank of these input parameters so that the most influential or dominant variables could be identified among the said input variables. The sensitivity analysis was carried out by using the Sobol method,[37] which is briefly described in the rest of this section. This methodology can be used to quantify the contribution of each input parameter to the variance of the output of the model. For a given output of the model, $f(x)$, the function may be decomposed as follows

$$
\begin{aligned}
f(x) = f_0 + \sum_{i=1}^{s} f_i(x_i) + \sum_{i=1}^{s}\sum_{i\neq j}^{s} f_{ij}(x_i, x_j) \\
+ \ldots + f_{1\ldots s}(x_1, x_2, \ldots, x_s)
\end{aligned}
\tag{5}
$$

Each term of the above decomposition can be expressed as the following integrals[49]

$$
\begin{aligned}
f_i(x_i) &= \int f(x) \prod_{k\neq i} dx_k - f_0 \\
f_{ij}(x_i, x_j) &= \int f(x) \prod_{k\neq ij} dx_k - f_0 - f_i(x_i) - f_j(x_j)
\end{aligned}
\tag{6}
$$

The above equations can only hold if the following orthogonality criterion is satisfied:

$$
\int f_{i1,\ldots,is}(x_{i1}, \ldots, x_{is}) dx_k = 0 \forall k = i_1, \ldots, i_s \tag{7}
$$

If equation (7) is satisfied, then one can assume that $f(x)$ is square-integrable (i.e., $f(x)$ can be squared and integrated), which also means that $f_{i1\ldots is}$ in equation (5) is also square-integrable. Squaring both sides of equation (5) and integrating yields

$$D = \sum_{i=1}^{k} D_i + \sum_{i<j} D_{ij} + \sum_{i<j<l} D_{ijl} + \ldots + D_{1,2,\ldots k} \quad (8)$$

where D is defined as the variance of the output, D_i is the partial variance corresponding to the subset of input i, D_{ij} is the partial variance corresponding to the subset of ij, and so on. The Sobol sensitivity indices can now be defined for each subset of individual parameters as

$$S_{i1,\ldots is} = \frac{D_{i1,\ldots,is}}{D} \quad (9)$$

Equation (9) is the ratio between the partial variance subsets with respect to the variance of the output of the model. These are called global sensitivity indices. The first-order sensitivity indices are the main effect of the individual parameters that are used to measure the fractional contributions due to a single parameter to the output variance. For example, $S_i = \frac{D_i}{D}$ would refer to the i^{th} input parameter's contribution to the output variance.

FE-based homogenization model for the effective elastic constant of SiCf/SiCm tube

The FE-based homogenization model has been used as a high-fidelity model and is discussed in this section. A multiscale homogenization was adopted in which a microscale homogenization predicts the effective elastic constants of SiC yarn from the mechanical properties of SiC fiber and SiC matrix, while a mesoscale homogenization was used to evaluate the effective elastic constants of the braided composite from the properties of yarn and matrix.

Microscale homogenization.

The SiC yarn is modeled as a transversely isotropic material having five independent elastic constants. The constitutive relationship of transversely isotropic material whose plane of symmetry is 1–2 is given by

$$\begin{Bmatrix} \sigma_{11} \\ \sigma_{22} \\ \sigma_{33} \\ \tau_{23} \\ \tau_{13} \\ \tau_{12} \end{Bmatrix} = \begin{bmatrix} C_{11} & C_{12} & C_{13} & 0 & 0 & 0 \\ C_{12} & C_{11} & C_{13} & 0 & 0 & 0 \\ C_{13} & C_{13} & C_{33} & 0 & 0 & 0 \\ 0 & 0 & 0 & C_{44} & 0 & 0 \\ 0 & 0 & 0 & 0 & C_{44} & 0 \\ 0 & 0 & 0 & 0 & 0 & \frac{C_{11}-C_{12}}{2} \end{bmatrix} \begin{Bmatrix} \varepsilon_{11} \\ \varepsilon_{22} \\ \varepsilon_{33} \\ \gamma_{23} \\ \gamma_{13} \\ \gamma_{12} \end{Bmatrix} \quad (10)$$

Thus, there are five independent stiffness coefficients for a transversely isotropic material. The evaluation of elastic constants from the stiffness tensor of equation (10) can be found be textbook resources.[50]

In this study, a hexagonal repeatable unit cell (RUC) was used as it captures the transversely isotropic nature of the unidirectional composite better than other types of RUCs.[51] The hexagonal RUC, shown in Figure S1 (in supplementary data), was modeled using the pre-processing features available in ABAQUS 2019 software. The fiber volume fraction within a yarn was assumed to be 52% as reported in the literature.[46] The pyrolytic carbon interface of the composite was not modeled in the current study as the analysis was in the linear elastic regime. The microporosity is assumed to be 12%. It is further assumed that the pores are trapped in the matrix. The Young's modulus and Poisson's ratio of the CVI SiC matrix at zero porosity were considered to be 438.80 GPa and 0.17, respectively,[52] which were used in equations (1) and (3) to account for microporosity. Young's modulus and Poisson's ratio of SiC fiber were 420 GPa and 0.18, respectively.[6] The outputs of microscale homogenization are the elastic constants of the SiC yarn. The relevant procedure and the boundary conditions can be found in other works.[53,54] The similar boundary conditions used in this study are shown in Table S1 (in supplementary data). The obtained effective elastic constants of yarn are now the input parameters in mesoscale FE-based homogenization discussed in the rest of this section.

Mesoscale homogenization.

In the mesoscale homogenization, the elastic constants of the textile composite are evaluated, knowing the elastic constants of the constituent SiC yarn and SiC matrix. It is not a straightforward process to obtain an FE model of the RUC of the textile composite due to the presence of undulating and interlacing yarns. The tubular specimen further adds to the complexity of the geometry. We use open-source TeXGen[55] software to generate the FE mesh of flat RUC of textile composite. The desired curved RUC is obtained by subsequent transformation of nodal coordinates of TeXGen generated FE mesh of flat RUC. The transformation procedure and the periodic boundary conditions imposed on the curved RUC can be found in the works of Nagaraju et al. [56] Another challenge with SiC_f/SiC_m composite tubes is that of a high yarn volume fraction of 67%. The modeling of such high yarn volume fraction composites can be cumbersome in TexGen software without yarn interpenetrations. This challenge was addressed by identifying the excess matrix elements in the FE model with a low yarn volume fraction and deleting them until the yarn volume fraction reached 67% in ABAQUS.[57] This FE model obtained by this heuristic approach is called the chipped-away model, schematically explained in Figure 2. The excessive matrix elements were

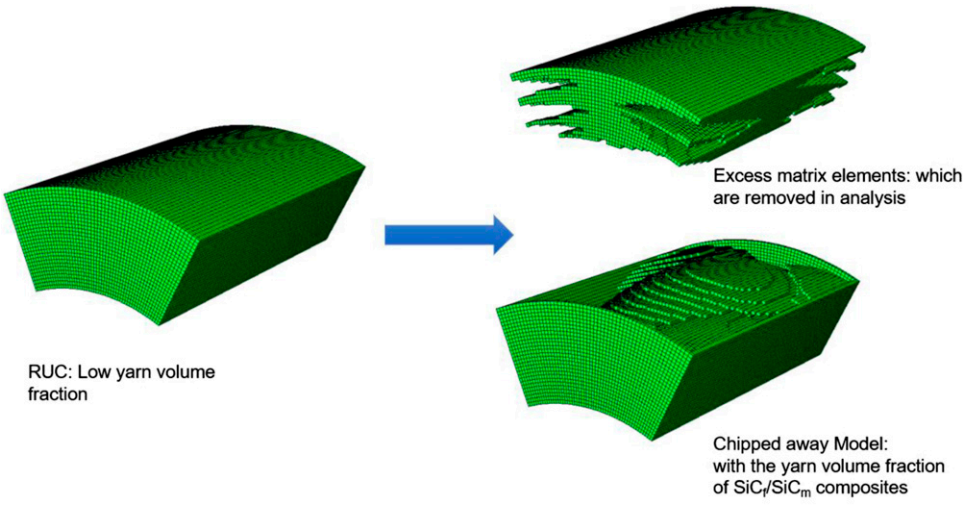

Figure 2. The schematic representation of the chipped-away model.

identified starting from the outer radius and removed until the yarn volume fraction becomes the desired value. The matrix elements on the boundary were not deleted as they are needed to specify the periodic boundary conditions. The effective elastic constants of the textile composite are then obtained by simulating three tests namely, the internal pressure test, longitudinal tensile test, and torsion test. In each of these tests, the periodic boundary conditions are imposed by using multi-point constraint equations in ABAQUS software. The complete details can be found in an earlier study[56] in which the relationship between macro-strains and micro-strains is shown to be

$$\varepsilon_\theta = \frac{R_m}{V}\sum_{e=1}^{n}\frac{\varepsilon_\theta^{(e)} v^{(e)}}{r^{(e)}} \tag{11}$$

where ε_θ is the macro-strain in the circumferential direction of the tube, R_m is the mean radius, V is the volume of the curved RUC $\varepsilon_\theta^{(e)}$, $v^{(e)}$, $r^{(e)}$ are the micro-strain, volume, and radius of the centroid of the finite element e, respectively, and n is the total number of elements in the FE model of the curved RUC.

The remaining strain components, ε_y (macro-strain in the longitudinal direction) and $\gamma_{\theta y}$ (torsional strain) can be calculated through similar formulae. The force resultants are obtained from the micro-stresses as

$$N_\theta = \frac{R_m}{A_m}\sum_{e=1}^{n}\frac{\sigma_\theta^{(e)} v^{(e)}}{r^{(e)}} \tag{12}$$

where N_θ is the force resultant along the circumferential direction and $A_m = 2\alpha L_y R_m$ is the area of the mid-surface of the curved RUC. Similar formulae hold to calculate the other force resultants N_y and $N_{\theta y}$. The Young's modulus along the circumferential direction (E_θ) was calculated in the FE simulation of the internal pressure test as

$$E_\theta = \frac{N_\theta}{\varepsilon_\theta t} \tag{13}$$

where ε_θ is the macro hoop strain is given by equation (11) and t is the thickness of RUC in the chipped-away model.

From the longitudinal tensile test, Young's modulus along the axis of the tube and the Poisson's ratio are calculated as:

$$E_y = \frac{N_y}{\varepsilon_y . t} \tag{14}$$

$$v_{\theta y} = \frac{-\varepsilon_\theta . t . E_\theta}{N_y} \tag{15}$$

Finally, the shear modulus is calculated from the FE simulation of the torsion test as

$$G_{\theta y} = \frac{N_{\theta y}}{\gamma_{\theta y}} \tag{16}$$

Thus, we can obtain the four elastic constants $(E_\theta, E_y, v_{\theta y}, G_{\theta y})$ for SiC$_f$/SiC$_m$ composite tubes accounting for the given information of residual porosity, curved geometry, and high yarn volume fraction.

Construction of polynomial response surface surrogate

A polynomial response surface (PRS) surrogate model is often desired for computationally intensive analyses. A PRS approximates the output of actual analysis through a linear combination of chosen monomials which are functions of

input variables. Suppose there are two input variables say x_1 and x_2, then one may select the PRS of the following form

$$\widehat{y} = \beta_0 + \beta_1 x_1 + \beta_2 x_2 + \beta_3 x_1 x_2 \tag{17}$$

where $\widehat{y}$ is the PRS prediction, and β_i are unknown coefficients. In matrix notation, the above equation can be rewritten as

$$\widehat{y} = \begin{bmatrix} 1 & x_1 & x_2 & x_1 x_2 \end{bmatrix} \begin{bmatrix} \beta_0 \\ \beta_1 \\ \beta_2 \\ \beta_3 \end{bmatrix} \tag{18}$$

The row vector $\begin{bmatrix} 1 & x_1 & x_2 & x_1 x_2 \end{bmatrix}$ is called the basis function. Suppose we have 10 samples i.e., ten realizations of input variables x_1, x_2 and the corresponding output from the actual analysis is y. Each of the ten samples could be arranged as follows

$$\begin{Bmatrix} y^{(1)} \\ y^{(2)} \\ . \\ y^{(10)} \end{Bmatrix} = \begin{bmatrix} 1 & x_1^{(1)} & x_2^{(1)} & x_1^{(1)} x_2^{(1)} \\ 1 & x_1^{(2)} & x_2^{(2)} & x_1^{(2)} x_2^{(2)} \\ . & . & . & . \\ 1 & x_1^{(10)} & x_2^{(10)} & x_1^{(10)} x_2^{(10)} \end{bmatrix} \begin{Bmatrix} \beta_0 \\ \beta_1 \\ \beta_2 \\ \beta_3 \end{Bmatrix} \tag{19}$$

In compact form, the above equation could be represented as

$$Y = X\beta \tag{20}$$

In the above equation X is called the design matrix or feature matrix. The vector of unknown coefficients β that minimize the squared sum of differences between the outputs of the actual analysis and PRS surrogates at the 10 training samples can be estimated by[58]

$$\beta = \left(X^T X\right)^{-1} X^T Y \tag{21}$$

The above solution is called the ordinary least square solution. In this study, the PRS surrogates have been constructed using the ordinary least square solution with appropriately chosen basis functions.

Uncertainty quantification

In this section, the procedure for quantifying uncertainty in elastic constants is explained. Although there are many methods available for uncertainty quantification (UQ), sampling-based methods are popular as they are independent of underlying distributions. The main challenge of sampling-based methods is that they require more than 10^5 samples to identify the distribution of a quantity of interest. A combined execution of FE-based microscale and macroscale homogenization took approximately 20 min on a computer with 32 GB of RAM equipped with an INTEL i7 processor. Thus, executing 10^5 FE simulations to generate sufficient sample data may not be computationally efficient. On the other hand, the low-fidelity analytical homogenization models are not sufficiently accurate enough. Hence, a natural alternative is to develop a fast-computing surrogate model based on several FE-based homogenization simulation results. Once a surrogate model with good prediction accuracy is developed, it can be invoked 10^5 times in Monte Carlo simulations (MCS) to generate the samples to identify the distribution.

In the current study, a PRS was built by using 30 samples of input variables, which were chosen based on the experimental design of Latin hypercube sampling (LHS). In the LHS method, the sample locations were distributed evenly over a sample space. A PRS with quadratic terms of the input variables was developed based on the ordinary least square solution. The performance of the PRS model was evaluated by calculating the predicted residual error sum of squares (PRESS), a form of cross-validation error. The prediction accuracy of the PRS surrogate was assessed by comparing the predictions of PRS with FE simulations at 8 different samples of input variables that were not used to calculate the regression coefficients. After confirming that the built PRS has a good predictive capability, it was used in MCS to generate 10^5 samples from which the distribution of effective elastic constants was identified, and uncertainty was quantified by calculating the coefficient of variation (CV). The CV is defined as the ratio of the standard deviation (σ) of the data to their mean (μ). The histogram plots of the data generated from MCS were used to identify the probability distribution that best fits the effective elastic constants of the composite tube. The detailed results are discussed in the next section.

Results and discussions

Verification of FE methodology

In this section, we will compare the prediction of the multiscale FE model discussed in Section 2.5 with the elastic constants of the SiC_f/SiC_m tube obtained through experiments. For this task, the mean values of elastic constants of SiC fiber and SiC matrix were considered, while overall porosity varied from 9% to 17% in increments of 2%. The chosen architecture was a 30° two-dimensional biaxial braided composite tube. As stated earlier, Young's modulus and Poisson's ratio of isotropic SiC fiber were 420 GPa and 0.17, respectively. Young's modulus of the SiC matrix at zero porosity was assumed to be 438.80 GPa.[52] The micro-porosity and yarn volume fraction were kept constant at the reported values of 12% and 67%,[46] respectively. The calculated elastic constants are graphically represented in Figure 3. From the literature for SiC_f/SiC_m composite tubes, the expected range of Young's modulus is

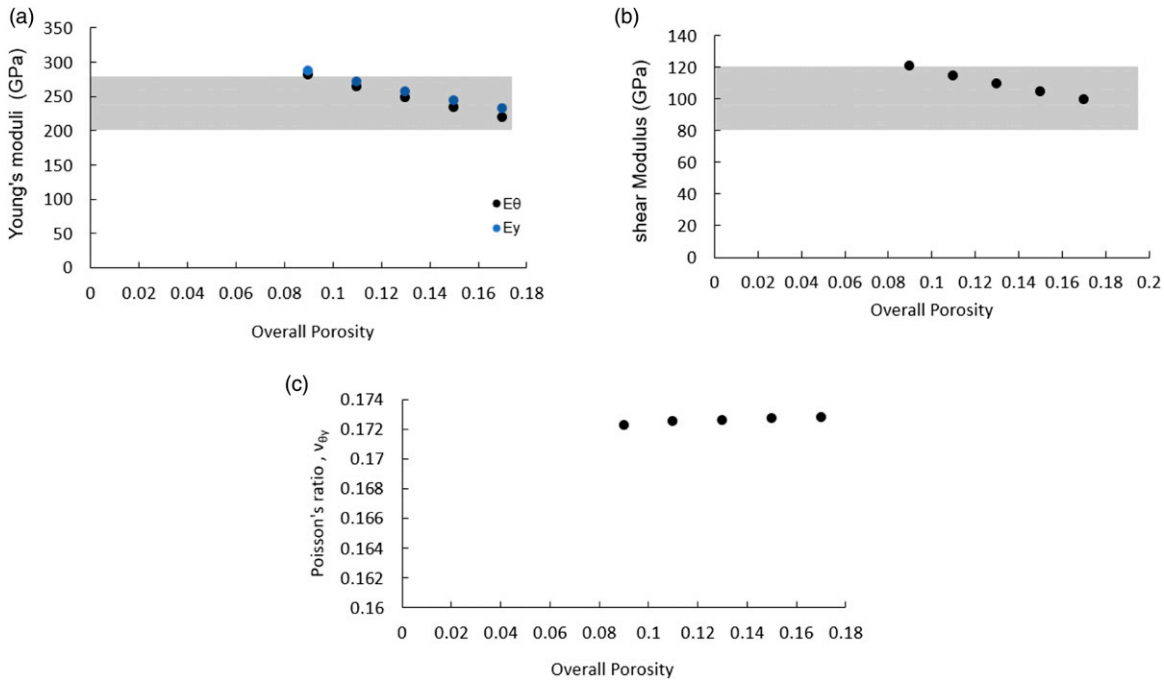

Figure 3. The elastic constants (Young's moduli in (a), shear modulus in (b), and Poisson's ratio in (c)) were calculated at mean values of material properties of SiC fiber and SiC matrix at different fractions of overall porosity. The shaded region denotes the experimental range.

200–280 GPa, the shear modulus is from 80–120 GPa and no data is available on the Poisson's ratio[7] of the composite tube. It can be observed from Figure 3, that the predictions of the chipped-away model are close to the range reported in experimental studies.[6,7] Thus, the chipped-away model has sufficient predictive capability to be used in subsequent analyses. It is to be noted that the methodology of calculation of elastic constants of SiC_f/SiC_m tubes was improvised to account for their unique characteristics such as residual porosity, high yarn volume fraction, and tubular geometry. It can be observed that Young's modulus of SiC_f/SiC_m tube is significantly lower than Young's modulus of constituent SiC fiber and SiC matrix at zero porosity.

Correlation between low-fidelity and high-fidelity models

The analytical model can provide the outputs quickly, but it is based on an assumption of averaging the stiffness methods which may not necessarily capture the physics accurately. The FE-based homogenization model, on the other hand, considers the characteristic features of textile composite through explicit/implicit modeling. However, the FE-based chipped-away model is computationally intensive. To determine the relative performance, the results of the low-fidelity BraidCAM model were compared with that of the high-fidelity chipped-away model as shown in Figure 4. It can be observed that there is a strong correlation between the results of the analytical model and the FE-based homogenization model. Although Poisson's ratio does not show a meaningful correlation, in general, its effect on homogenization is ignorable. Thus, it is possible to use the low-fidelity model to identify the dominant variables without any loss of accuracy as it gives the outputs much more quickly and it is easier to change the values of input variables in the low-fidelity model compared to the high-fidelity model.

Identification of dominant variables

Many manufacturing factors influence the uncertainty in the elastic constants of braided composite tubes. Among them, eight factors were selected based on our analysis of information available in the literature, which are summarized in Table S2 (in supplementary data) with their lower and upper bounds. Fiber volume fraction, yarn area, braiding angle, and Young's moduli of fiber/matrix were measured directly using conventional characterization techniques.[59] Poisson's ratio and porosity were based on literature.[7] Although all these variables can be used in uncertainty quantification, it would be computationally intensive to work with eight-dimensional space. This identification was done by global sensitivity analysis, using a PRS surrogate for the BraidCam model, involving identified eight input variables. Once a small number of significant input

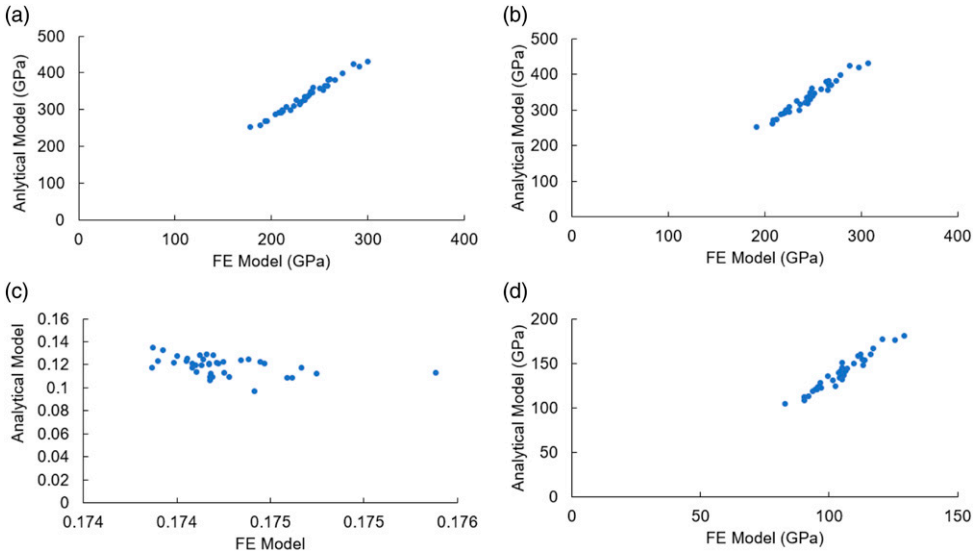

Figure 4. These graphs show a strong correlation between the results of the low-fidelity analytical model and the high-fidelity FE model. (a) Young's modulus along the circumferential direction, (b) Young's modulus along the longitudinal direction, (c) Poisson's ratio, and (d) shear modulus.

variables are identified, a more accurate surrogate model was generated using FE-based simulations in a lower-dimensional space. To construct the PRS surrogate, 34 samples were obtained from the LHS method. The PRS surrogate is useful to approximate the predictions of the BraidCAM analytical model. Instead of simulating millions of random realizations and then processing the results through BraidCAM, we can use a PRS as an approximation to mimic the results of BraidCAM while being computationally cheaper to evaluate. All input variables in Table S2 (in supplementary data) were normalized to be varying from 0 to 1, so that each input has the same weighting value in constructing the response surface of the following form

$$Y = \beta_0 + \beta_1 x_1 + \beta_2 x_2 + \ldots + \beta_8 x_8 \tag{22}$$

where β_i are the regression coefficients, x_i are the normalized input variables, and Y is the output of the response surface. The goodness of the fit equations was assessed by calculating the coefficient of determination, R^2. The summary of the statistics and the linear response surface coefficients are provided in Table 1. For all elastic constants, there exists a high coefficient of determination ($R^2 > 0.9$) with a low p-value (≈ 0) which indicates a strong linear relationship exists between the elastic constants and the chosen input variables for the multiple linear regression. Furthermore, the magnitude of the coefficients for each independent variable in Table 1 (β_i) represents the size of the effect that each variable has on the dependent variable. Across all elastic constants, the regression coefficient with the largest magnitude corresponds to the porosity (β_8) by a significant margin, followed by the elastic moduli of the constituents: SiC matrix (β_5) and SiC fiber (β_4).

The first-order Sobol indices were calculated using equation (9) and are summarized in Table 2. These indices represent the first-order effect that the desired input variable has on the output's variance. The Sobol indices were normalized such that they sum to one as shown in each row of Table 2. The larger the Sobol index, the greater the effect that the input variable has. The most significant contribution to the elastic constant variations is the porosity within the composite (S_8). This is followed by the elastic modulus of both the individual constituents (SiC matrix (S_5) and SiC fiber (S_4)). The rest of the variables do not play a significant role in comparison and therefore can be fixed at their mean value without affecting the uncertainty in the elastic constants of SiC_f/SiC_m tubular composites.

Quantification of uncertainty

The methodology to quantify uncertainty discussed in methodology is schematically shown in Figure 5. Having identified the three dominant variables influencing the elastic constants in the sensitivity study, we embark on building a more accurate PRS with a reduced number of input variables (Young's modulus of SiC fiber ($\tilde{x_1}$), Young's modulus of SiC matrix ($\tilde{x_2}$) and overall porosity ($\tilde{x_3}$)). The objective is to build a more accurate PRS with a reduced number of input variables which can be invoked 10^5 times during Monte-Carlo simulations. The FE analysis was executed at 38 realizations of dominant variables, out of which 30 sample points were chosen through LHS design,

Table 1. The polynomial response surface statistics and coefficients.

	R^2	β_0	β_1	β_2	β_3	β_4	β_5	β_6	β_7	β_8
E_y	0.9959	387.40	−2.18	−0.08	−0.40	4.95	25.07	0.22	1.01	−116.46
E_θ	0.9959	387.31	−2.16	−0.06	−0.19	4.94	25.06	0.20	1.01	−116.49
$G_{\theta y}$	0.9955	152.33	1.19	−0.04	−0.05	4.94	10.30	−0.13	0.41	−49.84
$v_{\theta y}$	0.9894	0.01	0.01	−0.001	−0.001	0.02	0.004	0.005	0.001	−0.021

Table 2. First-order Sobol indices.

	S_1	S_2	S_3	S_4	S_5	S_6	S_7	S_8
E_y	3.33×10^{-4}	1.13×10^{-5}	4.84×10^{-7}	0.002	0.044	3.41×10^{-6}	7.17×10^{-5}	0.9541
E_θ	3.28×10^{-4}	2.45×10^{-6}	2.79×10^{-7}	0.002	0.044	2.84×10^{-6}	7.15×10^{-5}	0.9542
$G_{\theta y}$	5.45×10^{-4}	7.94×10^{-7}	5.83×10^{-7}	0.009	0.041	6.31×10^{-6}	6.48×10^{-5}	0.9500
$v_{\theta y}$	0.193	4.16×10^{-5}	1.24×10^{-4}	0.331	0.019	2.53×10^{-4}	2.44×10^{-6}	0.456

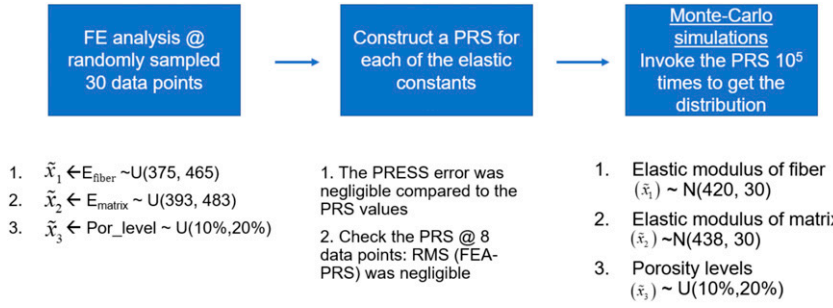

Figure 5. The approach to quantify uncertainty in elastic constants of SiC_f/SiC_m tube.

while 8 sample points that involved the lower and upper bounds of the dominant variables were additionally added to the dataset. In the LHS design, the combinations were sampled from uniform distributions of dominant variables. The associated lower and upper bounds are shown in Table S3 (in supplementary data).

These bounds were based on the values reported in the literature.[6,7,9] The uniform distribution along with the LHS method ensures that the selected combinations span the expected range of dominant variables and chosen values are not clustered close to each other. It can be observed that the order of Young's moduli is significantly different from that of overall porosity. Thus, the dominant variables were standardized by subtracting the mean from the values and subsequently dividing the difference by the standard deviation. The FE-generated data at 38 design of experiment (DOE) points were randomly split into a training set and a test set. The training set consisted of 30 instances of dominant input variables and corresponding FE results. A quadratic PRS of the following form was fit to the elastic constants by using the training set.

$$y = \beta_0 + \beta_1 x_1 + \beta_2 x_2 + \beta_3 x_3 + \beta_4 x_1 x_2 + \beta_5 x_1 x_3 + \beta_6 x_2 x_3 + \beta_7 x_1^2 + \beta_8 x_2^2 + \beta_9 x_3^2 \quad (23)$$

where y is the output response variable that denotes any of the four elastic constants of the SiC_f/SiC_m tube $(E_\theta, E_y, v_{\theta y}, G_{\theta y})$, x_i denote the standardized dominant variables, and β_i denote the regression coefficients that were calculated by the ordinary least square solution. The standardization of the dominant variables enables the comparison among the calculated regression coefficients. The PRS models were built separately for the 30° biaxial braided tube and the 45° biaxial braided tube. The regression coefficients of the two configurations are shown in Table 3 and Table S4 (in supplementary data), respectively. It can be observed that the regression coefficients associated with the quadratic monomials $(\beta_4 - \beta_9)$ are smaller compared to the coefficients associated with the linear monomials $(\beta_1 - \beta_3)$. It is further noted that the regression coefficient associated with the overall porosity (β_3) is highest in magnitude, followed by coefficients corresponding to Young's modulus of the

Table 3. The regression coefficients of equation (22) for 30° biaxial braided composite tubes.

Regression coefficients	$y = E_\theta$	$y = E_y$	$y = v_{\theta y}$	$y = G_{\theta y}$
β_0	234.31	244.98	0.174	104.61
β_1	4.53	6.44	1.07×10^{-4}	2.92
β_2	12.87	11.87	-1.02×10^{-4}	4.91
β_3	−26.31	−23.14	1.98×10^{-4}	−8.83
β_4	0.28	0.16	-8.47×10^{-5}	0.08
β_5	−0.27	−0.23	7.72×10^{-5}	−0.09
β_6	−1.65	−1.45	-7.13×10^{-5}	−0.56
β_7	−0.17	−0.10	4.35×10^{-5}	−0.05
β_8	−0.11	−0.05	2.81×10^{-5}	−0.03
β_9	1.54	1.44	3.25×10^{-6}	0.57

matrix (β_2) and that of the fiber (β_1). This trend is consistent with the Sobol indices discussed earlier.

The prediction accuracy of the surrogate model was assessed by calculating the PRESS. The PRESS measure is independent of the surrogate model. In the case of a PRS surrogate, the PRESS is given by

$$PRESS = \sqrt{\frac{1}{n_y - 1}\sum_{i=1}^{n_y}\left(\frac{e_i}{1 - H_{ii}}\right)^2} \tag{24}$$

where n_y is the number of training data points used in the regression process, e_i is the residual at i^{th} datapoint, calculated as the difference between predictions of FE simulations and PRS models, and H is defined as

$$H = X\left(X^T X\right)^{-1} X^T \tag{25}$$

where X is the design matrix, constructed such that row i is the instantiated values of the basis function of standardized dominant variables at i^{th} training data point. A surrogate model shows good fidelity when its PRESS value is close to zero. The PRESS values of PRS models of SiC_f/SiC_m tube are shown in Table S5 (in supplementary data). It is evident that the built PRS surrogates are a good fit by the low PRESS values. The prediction capability of the PRS models was assessed by comparing its prediction with FE simulations at eight points in the test set, which is disjoint from the training dataset. The root-mean-square (RMS) of difference in predictions of the FE model and surrogate model were calculated and are as shown in Table 4. The values in Table 4 are close to zero, which further confirms that the built PRS surrogates are capable of good predictions. The PRS models were used in MCS to identify the distribution of elastic constants.

In MCS, the distribution of the output quantity such as each of the elastic constants of the SiC_f/SiC_m tube can be identified if the distributions of the dominant variables are known. The assumed distributions of dominant variables were

Young's modulus of fiber – Normal (mean (μ) = 420 GPa, standard deviation (σ) = 30 GPa)
Young's modulus of matrix – Normal (mean (μ) = 438 GPa, standard deviation (σ) = 30 GPa)
Overall porosity – Uniform (Lower bound = 0.10, Upper bound = 0.20)

A sample point was randomly generated from these distributions and then standardized based on the corresponding mean and standard deviations used to determine the regression coefficients. The elastic constants were predicted by using appropriate PRS models at the sample point. This process was repeated 10^5 times to get the distribution of elastic constants. The histogram plots of 10^5 samples for each of the elastic constants are shown in Figure 6 and Figure S2 (in supplementary data) for 30° braided tubes, and 45° braided tubes respectively. It was found that a four-parameter Johnson distribution best fits the samples when compared to the typical two-parameter distributions such as uniform distribution, Gaussian distribution, lognormal distribution, and others. There are three families of Johnson distribution namely, S_L distribution, S_U distribution, and S_B distribution.[60,61] The data was such that the elastic constants were fit with bounded S_B Johnson distribution except for Poisson's ratio of 30° braided composites for which S_L Johnson distribution was a better approximation. In Johnson distribution, δ and γ are the shape parameters while ξ and λ are the location and scale parameters that correspond to the minimum value and range of data respectively. Additional information on Johnson distribution can be found in other works.[62] These values were found in the 'R' programming language by using the 'SuppDists' package.[63] The algorithm used the 5 order statistics of the data to find these parameter values. The Johnson distribution is a transformation of standard normal distribution defined by:

$$Z = \gamma + \delta\ \mathbf{log}(f(u)) \tag{26}$$

Table 4. The root-mean-square of the difference in predictions of FE simulations and PRS surrogate model.

Elastic constant	30° biaxial braided tube	45° biaxial braided tube
E_θ (GPa)	0.11	0.11
E_y (GPa)	0.10	0.11
$\nu_{\theta y}$	0.00	0.00
$G_{\theta y}$ (GPa)	0.04	0.05

Table 5. The parameters of Johnson distribution for the elastic constants of 30° braided composite tubes.

Parameters	E_θ	E_y	$\nu_{\theta y}$	$G_{\theta y}$
γ	0.3039	0.3452	0.0000	0.3916
δ	1.1107	1.2431	1.8543	1.3633
ξ	177	188	0.1738	81
λ	128	127	0.0004	54
Type	S_B	S_B	S_L	S_B

where $Z \sim N(0,1)$ and $u = \frac{x-\xi}{\lambda}$, x is a random variable and $f(u) = u$ for S_L Johnson distribution or

$f(u) = \frac{u}{1-u}$ for S_B Johnson distribution.

The Johnson parameters were as shown in Table 5 and Table S6 (in supplementary data) respectively for 30° and 45° braided SiC_f/SiC_m tubes. It is evident that fit parameters approximate the MCS-generated data as the blue curve in Figure 6 and Figure S2 closely follows the height of the histograms. The uncertainty in each of the elastic constants was quantified by calculating the coefficient of variation (CV) which is defined as the ratio of standard deviation to the mean of the concerned elastic constant. The higher the CV, the greater the uncertainty surrounding the mean of the elastic constant. The CV values calculated from the MCS-generated data are shown in Table 6. It can be noted that the CV values are about 10%, meaning that the elastic constants

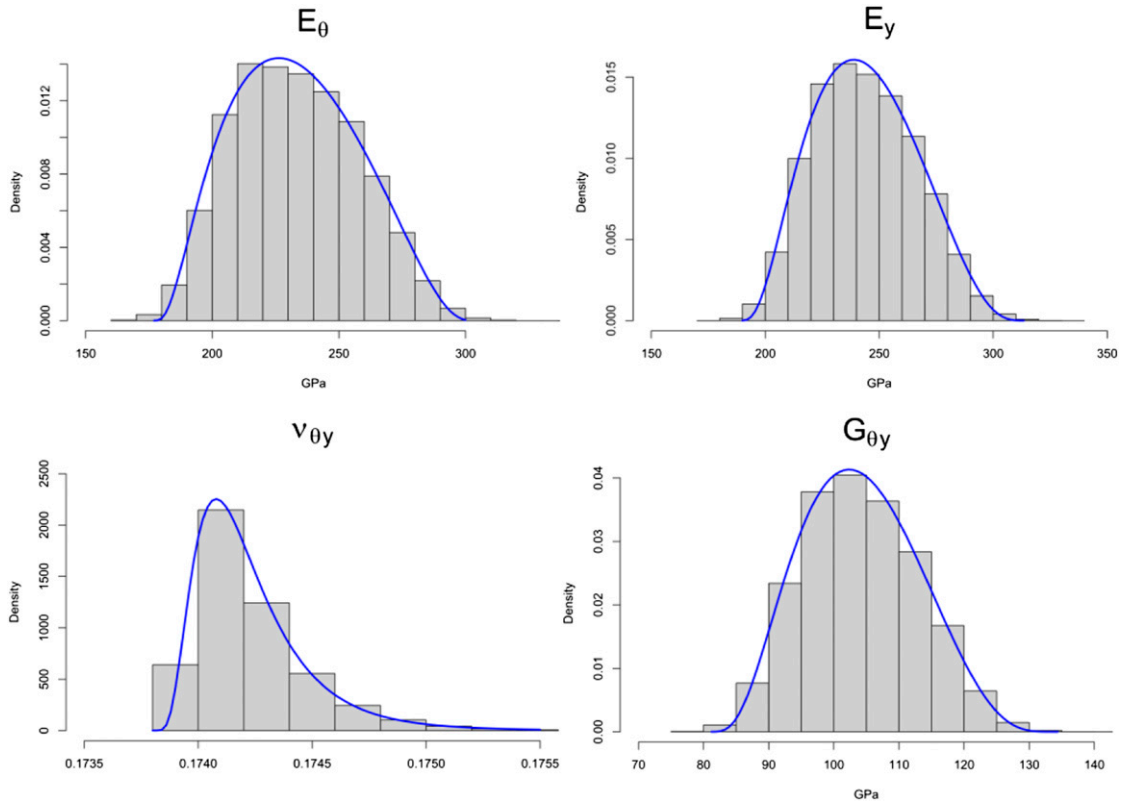

Figure 6. The histogram plots of elastic constants of 30° braided composite tubes. This data was obtained through MCS. The blue curve represents the Johnson distribution fit whose parameters are given in Table 5.

Table 6. The coefficient of variation (in %) of elastic constants from the MCS-generated data.

	30° braided composite	45° braided composite
E_θ	10.58	10.95
E_y	9.20	10.80
$\nu_{\theta y}$	0.14	1.93
$G_{\theta y}$	8.5	9.72

have a relatively lower spread around their mean values. The CV of Young's modulus of constituent materials (both SiC fiber and SiC matrix) is about 7.15% which only reached about 10% at the macroscale level of the composite tube. Finally, to further validate the approach adopted in the above analysis, we perform a similar analysis on a different composite and compare the results with those available in the literature. Singh et al. [40] evaluated the CV of elastic constant E_y of 55° triaxial braided SiC_f/SiC_m tubes through experiments carried out at different laboratories. A total of 43 samples were tested at 7 different laboratories. To compare the approach of this study with that of Singh et al., the RUC of 55° triaxial braided composite tube was considered. The uncertainty in elastic constant E_y of this tube was calculated as described in the current section. The mean value of the MCS-generated data of E_y was 236 GPa while the mean of E_y from the round-robin study of Singh et al. was 202 GPa. The CV from MCS-generated data was 10% compared to that of 20% reported in the round-robin study. In experiments, Singh et al. discussed that uncertainty involving the identification of linear elastic regime in the stress-strain plots of SiC_f/SiC_m tubes might have played a role in the calculation of CV. The measurement uncertainty often shows up in experimental studies. However, it was observed that the mean values of elastic constants of MCS-generated data from the current research study are in good agreement with the results in the round-robin study.[40]

Conclusions

An FE-based homogenization approach was discussed that predicts the elastic constants of SiC_f/SiC_m tubes. The Mori-Tanaka homogenization model was used to account for porosity which is easier than explicit modeling. The accuracy of the FE-based homogenization approach to calculate the elastic constants of SiC_f/SiC_m tubes was assessed by comparing its predictions with experimentally established ranges reported in the literature. Thus, the developed FE method is proven to predict the elastic constants of various architectures of SiC_f/SiC_m composites.

Through the global sensitivity analysis, it is demonstrated that Young's modulus of fiber, Young's modulus of the matrix, and residual porosity contribute significantly to the variation observed in the elastic constants of SiC_f/SiC_m composites. In this study, a linear polynomial expression was used as a surrogate for the BraidCAM model in sensitivity analysis while a quadratic polynomial expression was used as a surrogate for FE-based homogenization. The quadratic polynomial facilitated the quick generation of samples in the MCS. Based on the samples generated in MCS, it was found that the four-parameter Johnson distribution explains the statistics of the elastic constants of SiC_f/SiC_m composite tubes. The difference in parameters of Johnson distribution, for chosen 30° biaxial braided tubes and 45° biaxial braided tubes, is less than 10%. This study does not consider the interaction between porosity and braiding angle which can potentially lead to a greater difference in the parameters of Johnson distribution between 30° and 45° biaxial braided tubes. Based on the adapted computational framework in the sensitivity analysis, the braiding angle is not considered to be a key variable in determining the elastic constants of SiC_f/SiC_m composites.

Furthermore, in MCS the CV of constituent SiC fiber and SiC matrix was about 7%. This value is comparable to the CV of elastic constants of SiC_f/SiC_m tubes which is about 10%. This observation suggests that the variability in elastic constants of SiC_f/SiC_m tubes at the mesoscale is not significantly different from the CV observed at the microscale. Lastly, the parameters of the Johnson distribution that represent the statistics of elastic constants were reported, which could help model the performance of SiC_f/SiC_m cladding material.

Declaration of conflicting interests

The author(s) declared no potential conflicts of interest with respect to the research, authorship, and/or publication of this article.

Funding

The author(s) disclosed receipt of the following financial support for the research, authorship, and/or publication of this article: This work was supported by the Department of Energy (DOE) Nuclear Energy University Programs (NEUP) (grant no. DE-NE0008773).

Data availability

The raw/processed data required to reproduce these findings cannot be shared at this time due to technical or time limitations.

ORCID iD

Nam H Kim https://orcid.org/0000-0002-0221-9749

Supplemental Material

Supplemental material for this article is available online.

References

1. Djurovic B, Radjen S, Radenkovic M, et al. Chernobyl and Fukushima nuclear accidents: what have we learned and what have we done? *Vojnosanit Pregl* 2016; 73: 484–490.
2. Yun D, Lu C, Zhou Z, et al. Current state and prospect on the development of advanced nuclear fuel system materials: a review. *Mater Rep Energ* 2021; 1: 100007.
3. Kim HH, Kim JH, Moon JY, et al. High-temperature oxidation behavior of Zircaloy-4 and Zirlo in steam ambient. *J Mater Sci Technol* 2010; 26: 827–832.
4. Terrani KA, Zinkle SJ and Snead LL. Advanced oxidation-resistant iron-based alloys for LWR fuel cladding. *J Nucl Mater* 2014; 448: 420–435.
5. Terrani KA. Accident tolerant fuel cladding development: promise, status, and challenges. *J Nucl Mater* 2018; 501: 13–30.
6. Katoh Y, Ozawa K, Shih C, et al. Continuous SiC fiber, CVI SiC matrix composites for nuclear applications: properties and irradiation effects. *J Nucl Mater* 2014; 448: 448–476.
7. Koyanagi T, Katoh Y, Singh G, et al. SiC / SiC Cladding materials properties handbook. *ORNL/TM-2017/385, Prep US Dep energy Nucl Technol Res Dev Adv Fuels Campaign M3-FT17OR020202104, (Aug 2017)* 2017; 55.
8. Deck CP, Jacobsen GM, Sheeder J, et al. Characterization of SiC-SiC composites for accident tolerant fuel cladding. *J Nucl Mater* 2015; 466: 667–681.
9. Ichikawa H. Development of high performance SiC fibers derived from polycarbosilane using electron beam irradiation curing-a review. *J Ceram Soc Japan* 2006; 114: 455–460.
10. Roy S, Gebert JM, Stasiuk G, et al. Complete determination of elastic moduli of interpenetrating metal/ceramic composites using ultrasonic techniques and micromechanical modelling. *Mater Sci Eng A* 2011; 528: 8226–8235.
11. Wanner A. Elastic modulus measurements of extremely porous ceramic materials by ultrasonic phase spectroscopy. *Mater Sci Eng A* 1998; 248: 35–43.
12. Ziegler T, Neubrand A, Roy S, et al. Elastic constants of metal/ceramic composites with lamellar microstructures: finite element modelling and ultrasonic experiments. *Compos Sci Technol* 2009; 69: 620–626.
13. Karkkainen RL and Sankar BV. A direct micromechanics method for analysis of failure initiation of plain weave textile composites. *Compos Sci Technol* 2006; 66: 137–150.
14. Zhai J, Zeng T, Xu GD, et al. A multi-scale finite element method for failure analysis of three-dimensional braided composite structures. *Compos B Eng* 2017; 110: 476–486.
15. Yamada R, Igawa N, Taguchi T, et al. Highly thermal conductive, sintered SiC fiber-reinforced 3D-SiC/SiC composites: experiments and finite-element analysis of the thermal diffusivity/conductivity. *J Nucl Mater* 2002; 307–311: 1215–1220.
16. Chateau C, Gélébart L, Bornert M, et al. Micromechanical modeling of the elastic behavior of unidirectional CVI SiC/SiC composites. *Int J Sol Struct* 2015; 58: 322–334.
17. Meyer P and Waas AM. Mesh-objective two-scale finite element analysis of damage and failure in ceramic matrix composites. *Integr Mater Manuf Innov* 2015; 4: 63–80.
18. McLendon R and Whitcomb JD. Characteristic progressive damage modes in a plain weave textile composite under multiaxial loads. *J Compos Mater* 2017; 51: 1539–1556. DOI: 10.1177/0021998316662132.
19. Giselle Fernández-Godino M, Park C, Kim NH, et al. Issues in deciding whether to use multifidelity surrogates. *AIAA J* 2019; 57: 2039–2054.
20. Zhang Y, Kim NH, Park C, et al. Multifidelity surrogate based on single linear regression. *AIAA J* 2018; 56: 4944–4952.
21. Melchers RE. Importance sampling in structural systems. *Struct Saf* 1989; 6: 3–10.
22. Tokdar ST and Kass RE. Importance sampling: a review. *Wiley Interdiscip Rev Comput Stat* 2010; 2: 54–60.
23. Dey A and Mahadevan S. Ductile structural system reliability analysis using adaptive importance sampling. *Struct Saf* 1998; 20: 137–154.
24. Le Maître OP, Najm HN, Ghanem RG, et al. Multi-resolution analysis of Wiener-type uncertainty propagation schemes. *J Comput Phys* 2004; 197: 502–531.
25. Le Matre OP, Reagan MT, Najm HN, et al. A stochastic projection method for fluid flow: II. Random process. *J Comput Phys* 2002; 181: 9–44.
26. Goel T, Hafkta RT and Shyy W. Comparing error estimation measures for polynomial and Kriging approximation of noise-free functions. *Struct Multidiscip Optim* 2009; 38: 429–442.
27. Kersaudy P, Sudret B, Varsier N, et al. A new surrogate modeling technique combining Kriging and polynomial chaos expansions – application to uncertainty analysis in computational dosimetry. *J Comput Phys* 2015; 286: 103–117.
28. Crestaux T, Le Maître O and Martinez JM. Polynomial chaos expansion for sensitivity analysis. *Reliab Eng Syst Saf* 2009; 94: 1161–1172.
29. Bishop CM. Pattern recognition and machine learning. In: Jordan M, Kleinberg J and Schollkopf B (eds). Berlin, Germany: Springer, 2006. Epub ahead of print 2006. DOI: 10.1007/978-3-030-57077-4_11.
30. Saltelli A, Tarantola S, Campolongo F, et al. *Sensitivity analysis in practice: a guide to assessing scientific models*. Chichester, England: John Wiley & Sons, 2004.
31. Saltelli A. Sensitivity analysis: could better methods be used? *J Geophys Res* 1999; 104: 3789–3793.
32. McKay MD, Beckman RJ and Conover WJ. A comparison of three methods for selecting values of input variables in the analysis of output from a computer code. *Technometrics* 2000; 42: 55–61.
33. Cukier RI, Levine HB and Shuler KE. Nonlinear sensitivity analysis of multiparameter model systems. *J Comput Phys* 1978; 26: 1–42.

34. Saltelli A, Tarantola S and Chan P-S. A quantitative model-independent method for global sensitivity analysis of model output. *Technometrics* 1999; 41: 39–56.
35. Saltelli A and Sobol' IM. About the use of rank transformation in sensitivity analysis of model output. *Reliab Eng Syst Saf* 1995; 50: 225–239.
36. Archer GEB, Saltelli A and Sobol IM. Sensitivity measures, anova-like techniques and the use of bootstrap. *J Stat Comput Simul* 1997; 58: 99–120.
37. Sobol IM. Senstivity estimates for nonlinear mathematical models. *Math Model Comput Exp* 1993; 1: 407–414.
38. Santhosh U, Ahmad J, Ojard G, et al. Effect of porosity on the nonlinear and time-dependent behavior of ceramic matrix composites. *Compos Part B Eng* 2020; 184: 107658.
39. Gowayed Y, Ojard G, Prevost E, et al. Defects in ceramic matrix composites and their impact on elastic properties. *Compos Part B Eng* 2013; 55: 167–175.
40. Singh G, Gonczy S, Deck C, et al. Interlaboratory round robin study on axial tensile properties of SiC-SiC CMC tubular test specimens. *Int J Appl Ceram Technol* 2018; 15: 1334–1349.
41. Bernachy-Barbe F, Gélébart L, Bornert M, et al. Anisotropic damage behavior of SiC/SiC composite tubes: multiaxial testing and damage characterization. *Compos A Appl Sci Manuf* 2015; 76: 281–288.
42. Mura T. *Micromechanics of defects in solids*. Dordrecht, Netherlands: Springer. Epub ahead of print 1982. DOI: 10.1007/978-94-011-9306-1.
43. Eshelby JD. The determination of the elastic field of an ellipsoidal inclusion in an anisotronic medium. *Math Proc Cambridge Philos Soc* 1977; 81: 283–289.
44. Namet-Nasser S and Hori M. *Micromechanics: overall properties of heterogeneous materials*. Second Rev. Amsterdam, Netherlands: Elsevier B.V., 1999.
45. Becker F and Hopmann C. Stiffness estimates for composites with elliptic cylindrical voids. *Materials (Basel)* 2020; 13. Epub ahead of print 2020. DOI: 10.3390/ma13061354.
46. Rohmer E, Martin E and Lorrette C. Mechanical properties of SiC/SiC braided tubes for fuel cladding. *J Nucl Mater* 2014; 453: 16–21.
47. Melenka GW and Carey JP. Braid CAM: braided composite analytical model. *SoftwareX* 2018; 7: 23–27.
48. Melenka GW and Carey JP. Development of a generalized analytical model for tubular braided-architecture composites. *J Compos Mater* 2017; 51: 3861–3875.
49. Sobol IM. Global sensitivity indices for nonlinear mathematical models and their Monte Carlo estimates. *Math Comput Simul* 2001; 55: 271–280.
50. Gibson RF. *Principles of Composite Material Mechanics*. Boca Raton: CRC Press, 2016. Epub ahead of print 2016. DOI: 10.1201/b19626.
51. Li S. General unit cells for micromechanical analyses of unidirectional composites. *Compos Part A Appl Sci Manuf* 2001; 32: 815–826.
52. Gowayed Y, Ojard G, Miller R, et al. Mechanical properties of MI SiC/SiC composites and their constituents AFRL-ML-WP-TP-2007-472 (Preprint). https://www.researchgate.net/publication/235158219_Mechanical_Properties_of_MI_SiCSiC_Composites_and_Their_Constituents_Preprint
53. Zhu H, Sankar BV and Marrey RV. Evaluation of failure criteria for fiber composites using finite element micromechanics. *J Compos Mater* 1998; 32: 766–782.
54. Barbero EJ. *Finite element analysis of composite materials using abaqus*. Boca Raton, USA: CRC Press, 2013.
55. Lin H, Brown LP and Long AC. Modelling and simulating textile structures using texgen. *Adv Mater Res* 2011; 331: 44–47.
56. Thandaga Nagaraju H, Sankar BV, Subhash G, et al. Effect of curvature on extensional stiffness matrix of 2-D braided composite tubes. *Compos Part A Appl Sci Manuf* 2021; 147: 106422.
57. Element and contact pair removal and reactivation. https://abaqus-docs.mit.edu/2017/English/SIMACAEANLRefMap/simaanl-c-elemremovrepl.htm#simaanl-c-elemremovrepl-t-RemovingElements-sma-topic1 (2021, accessed 6 December 2021).
58. Myers RH, Montgomery DC and Anderson-cook CM. *Response surface methodology: process and product optimization using designed experiments*. 4th ed. New Jersey, USA: John Wiley & Sons, 2016.
59. Nance J. *Characterization of microstructural heterogeneity and mechanical properties of SiCf-SiCm composites*. University of Florida: Gainesville, USA, 2022.
60. Johnson NL. Bivariate distributions based on simple translation systems. *Biometrika* 1949; 36: 297–304.
61. Johnson ANL and Johnson BYNL. Biometrika trust systems of frequency curves generated by methods of translation Published by : Oxford University Press on behalf of Biometrika Trust Stable, 2020; 36: 149–176. URL: https://www.jstor.org/stable/2332539
62. Mateus A and Tomé M. Estimating the parameters of the Johnson's SB distribution using an approach of method of moments. *AIP Conf Proc* 2011; 1389: 1483–1485.
63. Wheeler B. SuppDists: Johnson function - RDocumentation, https://www.rdocumentation.org/packages/SuppDists/versions/1.1-9.7/topics/Johnson (accessed 1 November 2021).